HHS Public Access

Author manuscript

J Neural Eng. Author manuscript; available in PMC 2018 February 01.

Published in final edited form as:

J Neural Eng. 2017 February ; 14(1): 016016. doi:10.1088/1741-2552/aa5238.

Orientation Selective Deep Brain Stimulation

Lauri J Lehto[1], **Julia P Slopsema**[2], **Matthew D Johnson**[2], **Artem Shatillo**[3], **Benjamin A Teplitzky**[2], **Lynn Utecht**[1], **Gregor Adriany**[1], **Silvia Mangia**[1], **Alejandra Sierra**[3], **Walter C Low**[4], **Olli Gröhn**[1,3,‡], and **Shalom Michaeli**[1,‡,*]

[1]Center for Magnetic Resonance Research, University of Minnesota, 2021 6th St SE, Minneapolis, MN 55455, USA [2]Department of Biomedical Engineering, University of Minnesota, 312 Church St SE, Minneapolis, MN 55455, USA [3]A.I.Virtanen Institute for Molecular Sciences, University of Eastern Finland, Neulaniementie 1, FI-70211 Kuopio, Finland [4]Department of Neurosurgery, University of Minnesota, 2001 6th St SE, Minneapolis, MN, USA

Abstract

Objective—Target selectivity of deep brain stimulation (DBS) therapy is critical, as the precise locus and pattern of the stimulation dictates the degree to which desired treatment responses are achieved and adverse side effects are avoided. There is a clear clinical need to improve DBS technology beyond currently available stimulation steering and shaping approaches. We introduce orientation selective neural stimulation as a concept to increase the specificity of target selection in DBS.

Approach—This concept, which involves orienting the electric field along an axonal pathway, was tested in the corpus callosum of the rat brain by freely controlling the direction of the electric field on a plane using a three-electrode bundle, and monitoring the response of the neurons using functional magnetic resonance imaging (fMRI). Computational models were developed to further analyze axonal excitability for varied electric field orientation.

Main results—Our results demonstrated that the strongest fMRI response was observed when the electric field was oriented parallel to the axons, while almost no response was detected with the perpendicular orientation of the electric field relative to the primary fiber tract. These results were confirmed by computational models of the experimental paradigm quantifying the activation of radially distributed axons while varying the primary direction of the electric field.

Significance—The described strategies identify a new course for selective neuromodulation paradigms in DBS based on axonal fiber orientation.

Keywords

deep brain stimulation; orientation selective stimulation; fMRI; rat

[*]**Corresponding Author:** Name: Shalom Michaeli, University of Minnesota, Radiology Department, Center for MR Research 2021 6th St. SE Minneapolis, MN 55455, Phone: (612)-626-2001, shalom@cmrr.umn.edu, FAX: (612)-626-2004.

[‡]These authors are joint senior authors on this work

Introduction

Neuromodulation therapies that utilize electrical stimulation of deep brain structures have proved to be effective tools for managing a host of neurological and neuropsychiatric disorders [1]. With these therapies, spatiotemporal precision of stimulation often dictates if the desired treatment response is achieved and to what extent side effects are induced by stimulation. Targeting electrical stimulation selectively to key nodal pathways within the brain remains a challenging endeavor during deep brain stimulation (DBS). Recent attempts to improve the spatial selectivity of neuronal modulation with DBS have utilized high-field imaging to better localize deep brain structures [2, 3], smaller and more spatially distributed electrode sites [4–6], and advanced electrode stimulation configurations [7, 8].

While these approaches can help with defining the location of stimulation, there has been much less attention paid to spatial targeting based on the orientation of axonal fibers within a given region around the implanted electrodes. This challenge is significant as most clinical targets of DBS are embedded within complex networks of axonal fiber tracts with a range of local orientations and broadly distributed synaptic connections that when perturbed can result in inconsistent clinical outcomes across patients [9]. It is well known that the gradient of the extracellular electric field defines excitability of axons [10, 11]. Therefore, if the orientation of the gradient can be controlled, this will enable orientation selective stimulation of axonal populations. In structures where the neuronal ensemble of axonal fibers have a well-defined orientation, as in the corpus callosum (CC) or in other major white matter tracts in the brain, the maximal activation should thus occur with the electric field gradient oriented parallel to the orientation of the axonal track.

In this work, a new strategy for orientation-selective paradigms for DBS is presented, which is poised to increase precision of targeted activation beyond currently employed shaping and steering approaches. This was achieved using variable sets of amplitudes and a multichannel electrode configuration which enables control of the electric field direction in a plane and thus orient the spatial gradient of the electric field parallel to axonal tracts.

Materials and Methods

All surgical and experimental procedures were approved by the Institutional Animal Care and Use Committee (IACUC) of the University of Minnesota. Sprague-Dawley rats (Envigo; Madison, WI, USA; n = 12, male, 275–300 g) were initially anesthetized using isoflurane for the duration of the implantation (5% for induction, 2–3% during surgery) with O_2/N_2O 30%/70% carrier gas. Temperature was monitored with a rectal thermometer. The respiration rate was monitored with a plastic pressure sensor during the surgery and MRI. The temperature was maintained at 37 °C with a heating pad during the surgery and with heated water circulation and heated air during MRI. After the electrode implantation, the anesthesia was changed to urethane with three consecutive i.p. injections 15 minutes apart (1.25–1.50 g/kg) while gradually lowering the isoflurane level, reaching 0% after the last injection. We chose to use urethane as it enables a strong blood-oxygen-level dependent (BOLD) response [12, 13] and it is known to maintain near normal electrophysiology and blood gases in spontaneously breathing animals [14, 15].

The animal was placed on a stereotactic frame and a 1 mm craniectomy was performed on the right hemisphere through which a tripolar lead which is composed of a twisted set of three polyimide-insulated tungsten electrodes (PlasticsOne, MS333T/2C-A/SP; Roanoke, VA, USA) with tip-contact diameters of 200 μm were implanted in the CC (AP = −1.6 mm, ML = −2.5 mm, DV = −2.7 mm [16]). 3–4 drops of 2% lidocaine were administered before the incision of the scalp and before cauterizing vessels of the scalp and skull. For two animals in the second subgroup (see below), similar electrodes with tip-contact diameters 127 μm were used. The remaining hole in the skull around the electrode was filled with gelatin foam (SPONGOSTAN™, Søborg, Denmark). To fix the electrode, the hole was covered with dental acrylic (Lang Dental, Jet Acrylic, Wheeling, IL, USA). Finally, an Ag/AgCl wire (4 cm long, 0.5 mm diameter) acting as a ground electrode, was inserted below the skin with the tip ending at the base of the neck.

MRI was conducted in a horizontal 31 cm bore 9.4 T scanner equipped with Agilent (Palo Alto, CA, USA) DirectDRIVE console using a customized quadrature-loop radiofrequency transceiver designed for full rat brain coverage. Shimming was performed inside an approximately cerebrum sized voxel ($10 \times 10 \times 6.5$ mm^3) using a field mapping based shimming protocol included in the Agilent VNMRJ 4.0 package. Prior to fMRI, high resolution anatomical images were taken using fast spin-echo (FSE) pulse sequence with exactly the same slice positions: repetition time (TR) = 3 s, effective echo time (TE) = 48 ms, number of echoes = 8, matrix size = 256 × 256, field of view (FOV) = 25.6 × 25.6 mm^2, slice thickness = 1 mm and number of slices = 11. The fifth slice from the posterior was positioned at the center of the electrode. fMRI data was acquired with SE echo planar imaging with the following parameters: TR = 1.5 s, time resolution = 3 s (two excitations), number of volumes = 69, TE = 35 ms, matrix size = 64 × 64, FOV = 25.6 × 25.6 mm^2, slice thickness = 1 mm and number of slices = 11. Furthermore, to evaluate the directional distribution of axons in the target region of CC in detail, one additional rat brain was perfused, scanned with diffusion tensor imaging (DTI) and histologically stained for myelin [17]. DTI parameters using SE 3D readout were TR = 1 s, TE = 30 ms, 2 averages, acquisition bandwidth = 33.8 kHz, matrix size = 256 × 72 × 60, FOV = 2.93 × 1.65 × 1.37 cm^3, resolution after zero padding = 114^3 μm^3. Six diffusion directions were used so that Δ = 17 ms, δ = 5 ms, b = 1000 s/mm^2, and 1 acquisition without diffusion weighting.

The stimulation paradigm consisted of 60 s of rest and 18 s of stimulation, repeated twice and ending in a rest period. The stimulation waveforms were delivered using a digital-to-analogue converter (National Instruments; Austin, TX, USA) driven by MATLAB 2015b (Mathworks; Natick, MA, USA) and three stimulus-isolators (A-M Systems; Carlsborg, WA, USA). The placement of the electrode and the response of the brain to stimulus were confirmed by driving the tripolar electrode monopolar (i.e, biphasic, 60 μs per phase, 20 Hz, 0.4–0.6 mA) and by recording BOLD response in the somatosensory cortex (S1). During the experiments the performance of stimulus isolators were systematically monitored. For the directional stimulation, the relative current amplitudes $I_{1,2,3}$ of the three channels were chosen based on sinusoidal functions with phase offsets of 120° (Figure 1A, B) so that

$$I_1 = I_0 \sin(\phi)$$
$$I_2 = I_0 \sin(\phi + 120^\circ)$$
$$I_3 = I_0 \sin(\phi - 120^\circ),$$

where I_0 is the stimulation current amplitude and ϕ governs the stimulation angle. Sets of amplitudes were chosen in increments of 30° along the phase-offset sinusoids leading to 12 amplitude-combinations. This induced an electric dipole field such that the principal direction is defined by the phase step along the sinusoids (see Figure 1C). The order of fMRI trials with different directions of the stimulation was randomized for each experiment, and a 5 min break was taken between trials. Charge-balanced, symmetric biphasic 60 μs square pulses were delivered at a rate of 20 Hz. The pulse amplitude for the directional stimulation was 0.9 to 1.2 mA.

The analysis of the time series of fMRI data were performed using SPM8 (www.fil.ion.ucl.ac.uk/spm) and MATLAB. The preprocessing included slice timing correction, motion correction and spatial smoothing with a 2 × 2 full-width-at-half-maximum Gaussian kernel. The general linear model for SPM consisted of a block design model convolved with a rat hemodynamic function [18] and the baseline. For the statistical parametric maps, the significance threshold was set to $p < 0.05$ (family-wise error corrected). The maps were overlaid on the anatomical FSE images. The strength of the BOLD response with different stimulation directions was analyzed using a region of interest (ROI) drawn in the ipsilateral and contralateral barrel fields of the primary somatosensory cortex ($S1_{BF}$) in Aedes software package (aedes.uef.fi). The anatomically based ROIs were drawn on one or two EPI slices nearest to the electrode that showed activation with at least one stimulation angle. The mean time series were corrected for baseline and linear trending.

The 12 animals consisted of two non-random subgroups, in which the implanted orientation of the electrode was controlled or not. In the first subgroup of 6 rats the dependence of BOLD contrast on the orientation of the dipolar field within 0° to 360° was investigated without controlling the orientation of the implanted electrode. The angular dependence of the BOLD response was observed when the orientation of the dipolar field was varied. The maximal mean BOLD response averaged over 18 seconds after the BOLD contrast reached maximum during the first stimulus period, was assigned to the parallel orientation of the dipolar field with the axons of the CC, and designated as the 0° reference angle. For the second subgroup, the orientation of the lead tip was controlled using a microscope, identifying each channel with a multi-meter. Angle 0° was defined as the angle where cathode and anode point towards the ipsilateral and contralateral hemispheres, respectively. In both groups, ipsilateral and contralateral mean time series were then normalized to the ipsilateral mean maximum BOLD response to reduce the effects of inter-animal variability in BOLD contrast. Fitting a Gaussian function was used to estimate the deviation from the assumed angle of 0°, i.e., axons of the CC were assumed to travel exactly in the medial-lateral direction, however, this is not always the case (see Figure 5). Finally, the dependence of the activation on the stimulation angle was aggregated between two groups of rats.

Computational tissue conductance models were developed using COMSOL Multiphysics® v5.2 (COMSOL AB, Stockholm, Sweden) and were coupled with multi-compartment axonal models in NEURON v7.4 [19] to simulate the effects of the rotated dipole on radially distributed axons. The FEM model consisted of a 19 × 7.5 mm (length x radius) cylinder representing the approximate anatomical size of the rat brain [16]. The tissue was assumed to be homogeneous and isotropic with a conductivity of 0.11 S/m and relative permittivity of 30204, these values were calculated from the frequency dependent Cole-Cole dispersion function for gray matter described by Gabriel et al. using the median frequency component of a symmetric biphasic waveform (60 μs per phase, 7.197 kHz) [20]. The tripolar electrode configuration was modeled as three cylinders (200 μm diameter) positioned at the approximate experimental stereotactic location within the brain. The base of the brain cylinder furthest from the electrodes was set as ground to reflect the experimental setup, the electrode shafts were modeled as perfect insulators, and independent monopolar normal current densities were applied to the active disc surfaces on the tips of the electrodes.

The FEM model was solved for 24-amplitude combinations along the 120° phase-offset sinusoids using a Fourier FEM technique [21, 22]. For this method, the waveform (biphasic symmetric square pulse, 60 μs per phase, 1 ms length) was constructed, and the 1024-point discrete Fourier transform (DFT) of the stimulus waveform was used to transform the waveform from the time domain to the frequency domain. The FEM model was solved at 513 frequencies between 0 and 512 kHz. The resulting complex voltage distribution of the FEM was interpolated along straight multi-compartment 2 μm diameter myelinated axon models [23, 24]. Axon membrane dynamics were modeled using sodium and potassium channels, and passive leakage currents as described previously [24]. Axons were positioned at 12-orientations around the centroid of the three contact electrode in planes 0.2 to 1 mm below the surface of the electrodes (Figure 2A). The complex voltages were used to scale and shift the magnitude and phase of the frequency-domain waveform and the inverse DFT was applied to convert the extracellular voltage waveform back to the time-domain for each axon compartment. Stimulation waveforms were superimposed onto the model using the *e_extracellular* function in NEURON. Activation percentage curves were calculated by normalizing the angle between the primary direction of the electric field for a given amplitude combination and the orientation of each axon (Figure 2B). The percentage of activated axons (i.e. those with stimulus-entrained action potential activity) for each nominal stimulation angle was found using a stimulation of 1.2 mA and 60 radially distributed axons at 5 distances.

Results

The orientation of an electric field vector in a plane was controlled by inducing an electric dipole with a minimum of three electrode channels. The general concept for controlling the direction of an electric dipole using a tripolar electrode configuration is shown in Figure 1. Using amplitudes from phase offset sinusoidal functions (Fig. 1A, B) the anode and cathode can be shifted to rotate a dipole field (Fig. 1C). Figure 1D, E show that the electric field gradient of the dipolar field is greater when it is parallel to the principal electric field orientation as compared to the perpendicular direction, indicating that axons parallel to the dipole field should be excited at a lower threshold than perpendicular axons. By selecting the

amplitudes of the three channels from sinusoids with 120° phase offsets, one enables a rotation of the electric field below the tip of the electrode. To generate a uniform rotation with n channels the phase of the channel i should be defined as $360°/n*(i-1)$, given that the dipole is desired to be uniform in each direction.

As a proof of concept, the electrodes were implanted into the rat CC, and the response to stimulation was detected using simultaneous BOLD fMRI. The estimated standard deviation (SD) of the coordinates of implantation between animals obtained from anatomical images were: AP: −1.6 ± 0.4 mm, ML: −2.5 ± 0.5 mm, and DV: −2.7 ± 0.2 mm. Figure 3 shows a representative example of the fMRI activation map and averaged time courses (n = 12) from the rat brain. It can be seen from the time courses that the maximal amplitude of the BOLD response about the $S1_{BF}$ was detected when the electric field gradient was aligned with the fibers of the CC, while the activation was gradually reduced when the angle between the electric field and the fiber orientation was changed reaching a minimum at approximately 90° between the electric field gradient and the fibers. The BOLD contrast increased again gradually upon the re-orientation of the electric field to 180°, resulting again in a parallel orientation with the CC fiber pathway. The ratio of contralateral to ipsilateral activated pixels at the nominal stimulation angle 0° within the $S1_{BF}$ ROIs was 0.85 ± 0.65. In one out of 12 experiments contralateral activation was not observed.

In Figure 4A the averaged amplitudes of the normalized BOLD responses from ipsilateral and contralateral sides from 12 rats are shown. The angular dependencies of the BOLD were aligned from the independent experiments and averaged together. The figure demonstrates that maximal BOLD contrast was detected on both ipsilateral and contralateral sides for the angles 0° and 180° between the electric field and the neuronal track in the CC, while reaching minima for the angles 90° and 270°. Notably, the mean of the BOLD contrast was not statistically significantly smaller when the dipole was oriented at 180° to axons in the CC as compared to the BOLD contrast at 0° (Figure 4A, B).

To further support our experimental findings, a computational model was developed to demonstrate the dependence of axonal activation on the angle between the primary direction of the electric field and axons radially distributed below the plane of the electrodes (Figure 2, Figure 4C). The peak activation percentage was 80% for nominal stimulation angles of 0° and 180°, when the electric field was oriented parallel to the axons of the CC. The activation percentage decreased as the angle between the axon and the electric field increased, with minimum activation percentages of 18.33% and 16.67% at angles of 90° and 270° respectively, when the electric field was oriented perpendicular to the axons. The orientation dependence of the model was sharper compared to the experimental results.

In four rats within the group of six, the maximal BOLD contrast was detected when the angles were 16° ± 17° from the visually determined axial plane. These findings are in good agreement with orientation of the fiber tracts in the CC, which varies within ~30° from the anterior-posterior direction when moving to the deep areas of CC from cortex (Figure 5). In two rats out of six, the maximal BOLD contrast was instead detected at 102° and 92°. Even though all animals showed activation in $S1_{BF}$, also other cortical areas were indeed occasionally stimulated, such as retrosplenial/cingulate ($Cg_{1/2}$; n = 3) and S1 forelimb/

hindlimb ($S_{1FL/HL}$; n = 4) cortices. Three examples of the activation pattern variability are shown in Figure 6. To investigate the orientation dependence of the activation outside $S1_{BF}$, an additional ROI analysis was conducted in these regions and the results are summarized in Table 1 (see ROIs in Figure 6C). It should be noted that the ipsilateral and contralateral $Cg_{1/2}$ ROIs were not defined separately because of insufficient image resolution, and thus were averaged together. Similarly, while activation was also detected in motor cortex, reliable assignment was not possible and thus motor cortex was excluded from our analysis. Although peak BOLD responses were different at the nominal stimulation angles 0°, 90°, 180° and 270° for each ROI, only activation in the $S1_{BF}$ area was significantly greater for the stimulation angles 0° and 180° as compared to the minimal values observed for 90° and 270°.

Discussion

In this work, a new strategy for orientation-selective paradigms for DBS was developed and whole brain activation response was monitored using BOLD fMRI. The method aims at increasing precision of targeted activation beyond currently employed shaping and steering approaches [4–8]. This was achieved using a multichannel electrode configuration and variable sets of amplitudes based on sinusoidal functions with 120° phase offsets, which enabled control of the orientation the spatial gradient of the electric field dipole. It is noteworthy that the dipole field and its derivatives maintain their shape regardless of the orientation relative to the electrode, even though the electrode design is in its simplest 3-channel configuration.

The activation detected in rat's brain area $S1_{BF}$ exhibited dramatic dependence on the orientation of electric field gradient generated from the tripolar electrode implanted in the CC. Activation was also seen outside of $S1_{BF}$, however, the activated regions did not exhibit pronounced stimulation orientation dependence although it could be achieved with a different electrode placement. These activation patterns could be attributed to suboptimal electrode placement and also to the stimulation of the adjacent tracks with anterior-posterior orientation of the fibers. Whereas we did our best to guarantee reproducible electrode placement, partial inaccuracy of the electrode implantation (e.g., slight tilt of the implanted electrode or location of the tip of the lead) could not be avoided. A more refined study with larger number of channels of the lead could overcome imperfection of electrode placement and increase precision of the stimulation.

The computational models supported our experimental results of maximum activation for parallel axon orientations, and minimum activation for perpendicular axon orientations relative to the electric field orientation. The simulation results demonstrated sharper dependence of the activated axons on the orientation angle as compared to the experiment. We attribute this to the smoothing of the angular dependence during fMRI due to the distribution of the electric field dipole and due to a greater stimulation angle step (30°) for the experimental setup compared to simulations (15°). It is also noteworthy, that the activation percentages of the simulated axons were not zero at nominal stimulation angles of 90° and 270°. No activation would be expected for an axon traveling through the center of a dipole field perpendicular to the primary axis because the surface of zero extracellular

electric potential is planar. However, in the tripolar electrode, when all channels are conducting, two channels share one pole of the dipole field, indicating that the dipole is asymmetric and thus the surface of zero electric potential is not planar but curved. Therefore, the straight axon positioned under the center of the tripolar electrode perpendicular to this asymmetric dipole experiences a non-zero spatial derivative of the electric field and thus can be activated. Finally, possible curvature of real axons can lead to strong spatial derivatives of the electric field along the axons thus creating hotspots for inducing action potentials [25, 26].

The effect of having a parallel bipolar electrode configuration perpendicular and parallel to axons has been studied by stimulating the rat midbrain [27, 28] with seemingly contradictory results to those presented here. Using 60 Hz sinusoidal stimulation, the forepaws response was detected at lower thresholds when the electrodes, or dipole, were perpendicular to the target axons compared to a parallel orientation [28]. The same authors showed later with electrodes parallel to the axons, but by using 200 μs square pulses at 200 Hz instead of sinusoids, that the stimulation was significantly less dependent on the electrode orientation [28]. It was concluded that the sinusoidal pulses that were used previously led to an anodic block, inhibiting the action potential from traveling to the brain in the parallel orientation [29], whereas when using the square pulses, the pulse length was not long enough to form a block. The anodic block was also demonstrated in the hypothalamus by changing the polarity of a bipolar electrode parallel to the axons, so that a response was seen when the cathode was towards the frontal brain [30]. Based on these findings, a full anodic block was unlikely for our stimulation paradigm. Additionally, contrary to Szabo et al., our results showed clear orientation dependence. We attribute this difference to longer, 200 μs pulses and tenfold, 200 Hz stimulation rate used by Szabo et al. (in our case, 60 μs and 20 Hz).

Previously, orientation selective DBS has been studied for axons perpendicular and parallel to DBS leads with high-perimeter cylindrical electrodes [31] and with cylindrical electrodes with different height to diameter ratios [32]. Both studies showed that selectivity can be achieved with cylindrical electrodes, and that longer electrodes are more selective to axons perpendicular to the lead, while shorter electrodes are more selective to the parallel axons. This can be explained with the second spatial derivative of the electric potential, so that the electric field potential of a long electrode is more homogeneous parallel to the electrode orientation leading to a smaller second spatial derivative as compared to the perpendicular direction, and vice versa for the short electrodes. Selectivity to parallel axons was also achieved with an asymmetric bipolar electrode and a cathodic electrode surrounded by anodes [32]. Although those results are very encouraging, the control of orientational selectivity of the lead is restricted by the orientation in which the lead is implanted. On the other hand, the present study demonstrates that an electrode design with multiple and independently driven channels inherently provides flexibility in orienting the electric field in space irrespective of the orientation of electrode implantation, and ultimately leads to various degrees of neuronal stimulation.

As shown in Figure 2, three, or more, channels could also be used to create rotating, rather than static-orientation electrical fields. When the trajectory of the stimulating field covers all

directions evenly in time, the electric field will evenly stimulate all cells whose axonal orientations lie within the orientation space of the electric field. This may provide an efficient and robust stimulation approach for grey matter or in situations when it is desirable to simultaneously stimulate multiple fiber populations with different orientations. Furthermore, the approach enables a versatile design of electric field trajectories which can be optimized to selectively stimulate one or more axonal populations.

Finally, MRI pulse sequences can induce unwanted currents in DBS leads. This can cause heating of the tip of the electrode [33, 34]. However, tissue damage has not been reported so far in previous DBS-fMRI studies in rats [35–37]. In our experiments based on scout MRI tests conducted during and at the end of the studies, we did not notice any tissue damage. It is also possible that induced currents would cause neuromodulation themselves. Peripheral nerve stimulation is a possible side effect of MRI, however, to the best of our knowledge the brain stimulation during DBS just by MRI pulse sequences have not been reported.

Conclusion

To summarize, the concept of selectivity of neuromodulation based on the angular dependence of axonal excitability was evaluated using a directional electric field approach for stimulation. It was shown that biphasic pulses with amplitudes chosen independently for each channel of an electrode based on sine functions with constant phase offsets enabled orientation selective electric stimulation. The orientation selectivity was implemented using tripolar electrodes implanted into the rat CC where fiber orientation is well defined. Computational models demonstrated angular dependence of the excitability of axons with respect to the orientation of the stimulating electric field, supporting the experimental findings. To the best of our knowledge, this is the first demonstration of orientation selectivity created using multichannel electrodes for DBS applications as detected using fMRI.

Acknowledgments

The Office Technology Commercialization (OTC) of the University of Minnesota filed provisional application N# ROI20150170, LJ Lehto, A Shatillo, S Mangia, M Johnson, O Gröhn and S Michaeli, *Deep brain stimulation system that generates rotating or spatially selective electromagnetic fields*. This work was supported by the following sources: NIH grants: P41-EB015894, P30-NS057091; UEF-Brain Pool; R01-NS081118; R01-NS094206; Michael J Fox Foundation; Fulbright-Saastamoinen Foundation Grant in Health and Environmental Science to SM; MnDRIVE post-doctoral fellowship to LJL; and NSF IGERT fellowship (DGE-1069104) to JPS; Academy of Finland. This project has received funding from the European Union's Horizon 2020 research and innovation programme under the Marie Skłodowska-Curie grant, agreement No 691110 (MICROBRADAM).

References

1. Johnson MD, et al. Neuromodulation for brain disorders: challenges and opportunities. IEEE Trans Biomed Eng. 2013; 60(3):610–24. [PubMed: 23380851]
2. Abosch A, Yacoub E, Ugurbil K, Harel N. An assessment of current brain targets for deep brain stimulation surgery with susceptibility-weighted imaging at 7 tesla. Neurosurgery. 2010; 67(6): 1745–56. discussion 1756. [PubMed: 21107206]
3. Duchin Y, Abosch A, Yacoub E, Sapiro G, Harel N. Feasibility of using ultrahigh field (7 T) MRI for clinical surgical targeting. PLoS One. 2012; 7(5):e37328. [PubMed: 22615980]

4. Martens HC, Toader E, Decre MM, Anderson DJ, Vetter R, Kipke DR, Baker KB, Johnson MD, Vitek JL. Spatial steering of deep brain stimulation volumes using a novel lead design. Clin Neurophysiol. 2011; 122(3):558–66. [PubMed: 20729143]
5. van Dijk KJ, Verhagen R, Chaturvedi A, McIntyre CC, Bour LJ, Heida C, Veltink PH. A novel lead design enables selective deep brain stimulation of neural populations in the subthalamic region. J Neural Eng. 2015; 12(4):046003. [PubMed: 26020096]
6. Connolly AT, et al. A Novel Lead Design for Modulation and Sensing of Deep Brain Structures. IEEE Trans Biomed Eng. 2016; 63(1):148–57. [PubMed: 26529747]
7. Chaturvedi A, Foutz TJ, McIntyre CC. Current steering to activate targeted neural pathways during deep brain stimulation of the subthalamic region. Brain Stimul. 2012; 5(3):369–77. [PubMed: 22277548]
8. Butson CR, McIntyre CC. Role of electrode design on the volume of tissue activated during deep brain stimulation. J Neural Eng. 2006; 3(1):1–8. [PubMed: 16510937]
9. Riva-Posse P, et al. Defining critical white matter pathways mediating successful subcallosal cingulate deep brain stimulation for treatment-resistant depression. Biol Psychiatry. 2014; 76(12): 963–9. [PubMed: 24832866]
10. Rattay F. Analysis of models for external stimulation of axons. IEEE transactions on biomedical engineering. 1986; (10):974–977. [PubMed: 3770787]
11. Rattay F. Analysis of models for extracellular fiber stimulation. IEEE Trans Biomed Eng. 1989; 36(7):676–82. [PubMed: 2744791]
12. Kwong KK, et al. Dynamic magnetic resonance imaging of human brain activity during primary sensory stimulation. Proc Natl Acad Sci U S A. 1992; 89(12):5675–9. [PubMed: 1608978]
13. Ogawa S, Tank DW, Menon R, Ellermann JM, Kim SG, Merkle H, Ugurbil K. Intrinsic signal changes accompanying sensory stimulation: functional brain mapping with magnetic resonance imaging. Proc Natl Acad Sci U S A. 1992; 89(13):5951–5. [PubMed: 1631079]
14. Huttunen JK, Grohn O, Penttonen M. Coupling between simultaneously recorded BOLD response and neuronal activity in the rat somatosensory cortex. Neuroimage. 2008; 39(2):775–85. [PubMed: 17964186]
15. Paasonen J, Salo RA, Shatillo A, Forsberg MM, Narvainen J, Huttunen JK, Grohn O. Comparison of seven different anesthesia protocols for nicotine pharmacologic magnetic resonance imaging in rat. Eur Neuropsychopharmacol. 2016; 26(3):518–31. [PubMed: 26796682]
16. Paxinos, G., Watson, C. The Rat Brain in Stereotaxic Coordinates. 5th. Elsevier Academic Press; Amsterdam Boston: 2005.
17. Laitinen T, Sierra A, Bolkvadze T, Pitkanen A, Grohn O. Diffusion tensor imaging detects chronic microstructural changes in white and gray matter after traumatic brain injury in rat. Front Neurosci. 2015; 9:128. [PubMed: 25954146]
18. Silva AC, Koretsky AP, Duyn JH. Functional MRI impulse response for BOLD and CBV contrast in rat somatosensory cortex. Magn Reson Med. 2007; 57(6):1110–8. [PubMed: 17534912]
19. Carnevale, NT., Hines, ML. The NEURON book. Cambridge University Press; 2006.
20. Gabriel S, Lau RW, Gabriel C. The dielectric properties of biological tissues: III. Parametric models for the dielectric spectrum of tissues. Phys Med Biol. 1996; 41(11):2271–93. [PubMed: 8938026]
21. Butson CR, McIntyre CC. Tissue and electrode capacitance reduce neural activation volumes during deep brain stimulation. Clin Neurophysiol. 2005; 116(10):2490–500. [PubMed: 16125463]
22. Yousif N, Bayford R, Liu X. The influence of reactivity of the electrode-brain interface on the crossing electric current in therapeutic deep brain stimulation. Neuroscience. 2008; 156(3):597–606. [PubMed: 18761058]
23. McIntyre CC, Mori S, Sherman DL, Thakor V, Vitek JL. Electric field and stimulating influence generated by deep brain stimulation of the subthalamic nucleus. Clin Neurophysiol. 2004; 115(3): 589–95. [PubMed: 15036055]
24. McIntyre CC, Richardson AG, Grill WM. Modeling the excitability of mammalian nerve fibers: influence of afterpotentials on the recovery cycle. J Neurophysiol. 2002; 87(2):995–1006. [PubMed: 11826063]

25. Rattay F, Minassian K, Dimitrijevic MR. Epidural electrical stimulation of posterior structures of the human lumbosacral cord: 2. quantitative analysis by computer modeling. Spinal Cord. 2000; 38(8):473–89. [PubMed: 10962608]
26. Eickenscheidt M, Zeck G. Action potentials in retinal ganglion cells are initiated at the site of maximal curvature of the extracellular potential. J Neural Eng. 2014; 11(3):036006. [PubMed: 24762943]
27. Szabo I, Milner PM. Self-stimulation in rats: tip alignment influences the effectiveness of bipolar electrodes. Brain Res. 1972; 48:243–50. [PubMed: 4645207]
28. Szabo I, Milner PM. Electrode tip alignment and self-stimulation: influence of anodal hyperpolarization. Physiol Behav. 1973; 11(4):581–3. [PubMed: 4582676]
29. Van Den Honert C, Mortimer JT. Generation of unidirectionally propagated action potentials in a peripheral nerve by brief stimuli. Science. 1979; 206(4424):1311–1312. [PubMed: 515733]
30. Szabo I, Nad E, Szabo C. Pole reversals and hypothalamic self-stimulation: ascending spread of rewarding excitation. Physiol Behav. 1972; 9(2):147–50. [PubMed: 4569942]
31. Howell B, Grill WM. Evaluation of high-perimeter electrode designs for deep brain stimulation. Journal of neural engineering. 2014; 11(4):046026. [PubMed: 25029124]
32. Howell B, Huynh B, Grill WM. Design and in vivo evaluation of more efficient and selective deep brain stimulation electrodes. Journal of neural engineering. 2015; 12(4):046030. [PubMed: 26170244]
33. Shrivastava D, Abosch A, Hanson T, Tian J, Gupte A, Iaizzo PA, Vaughan JT. Effect of the extracranial deep brain stimulation lead on radiofrequency heating at 9.4 Tesla (400.2 MHz). J Magn Reson Imaging. 2010; 32(3):600–7. [PubMed: 20815057]
34. Shrivastava D, Abosch A, Hughes J, Goerke U, DelaBarre L, Visaria R, Harel N, Vaughan JT. Heating induced near deep brain stimulation lead electrodes during magnetic resonance imaging with a 3 T transceive volume head coil. Phys Med Biol. 2012; 57(17):5651–65. [PubMed: 22892760]
35. Lai HY, Albaugh DL, Kao YC, Younce JR, Shih YY. Robust deep brain stimulation functional MRI procedures in rats and mice using an MR-compatible tungsten microwire electrode. Magn Reson Med. 2015; 73(3):1246–51. [PubMed: 24798216]
36. Lai HY, Younce JR, Albaugh DL, Kao YC, Shih YY. Functional MRI reveals frequency-dependent responses during deep brain stimulation at the subthalamic nucleus or internal globus pallidus. Neuroimage. 2014; 84:11–8. [PubMed: 23988274]
37. Yang PF, Chen YY, Chen DY, Hu JW, Chen JH, Yen CT. Comparison of fMRI BOLD response patterns by electrical stimulation of the ventroposterior complex and medial thalamus of the rat. PLoS One. 2013; 8(6):e66821. [PubMed: 23826146]

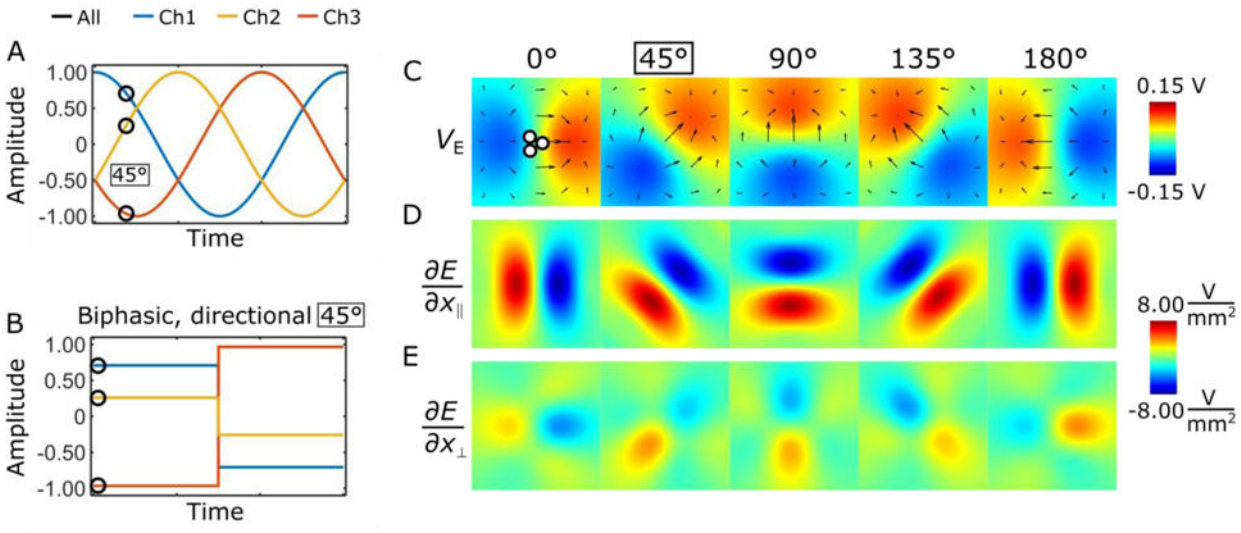

Figure 1.

Rotating and directionally selective electric fields generated using a tripolar electrode configuration. The electric field rotation can be produced using sinusoid waveforms (A), or the electric field can be fixed by selecting individual pulse amplitudes for each channel (B). The induced electric field potentials, and the electric field gradients parallel and perpendicular the electric dipole field are shown in (C-E), respectively.

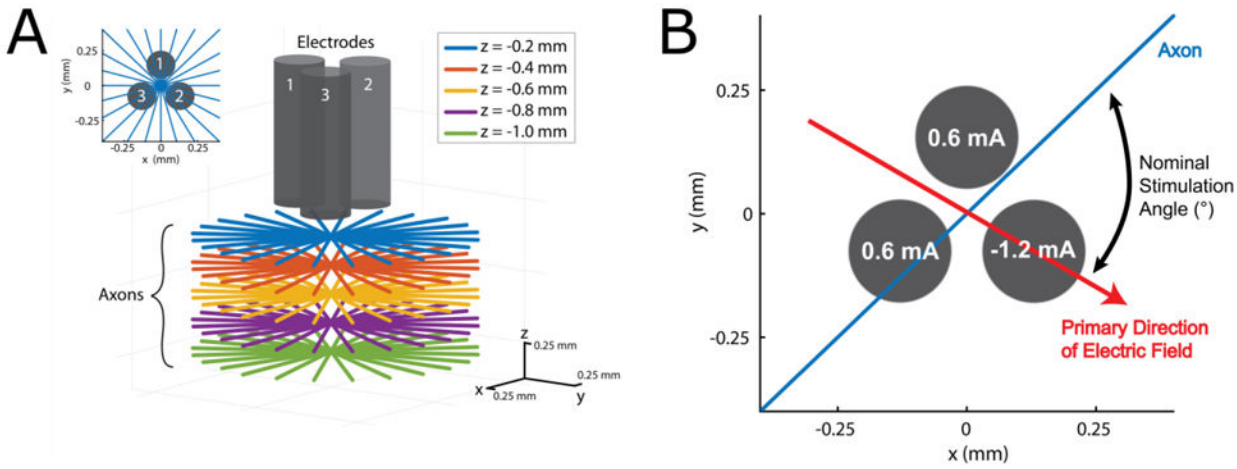

Figure 2.

Schematic representation of the simulation setup. (A) Axon placement: 12 axons were radially distributed around the centroid of the electrodes in 5 planes 0.2 to 1 mm below the electrodes. (B) The nominal stimulation angle was calculated as the angle between the primary direction of the dipole for a given amplitude combination and the orientation of the axon, this example has a nominal stimulation angle of 75°.

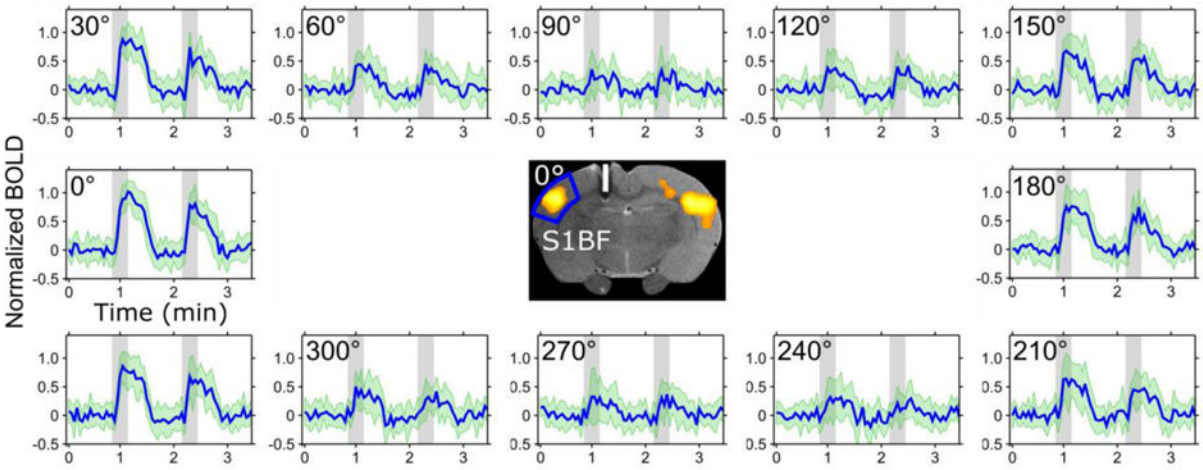

Figure 3.

Activation resulting from directionally selective biphasic pulses applied in the CC in the rat brain. Time series averaged over 12 animals for different orientations of the electric field relatively to the axonal track in the CC. When the principal direction of the dipolar field was orientated at 90° and 270° relative to the axonal track, no BOLD contrast was observed during the stimulation. The ROI for the time series is shown in the middle with a representative BOLD activation map at 0° overlaid on a FSE image where the white bar represents an estimate of the electrode dimensions and placement in the brain based on Paxinos' rat atlas [16]. The SDs are indicated in green.

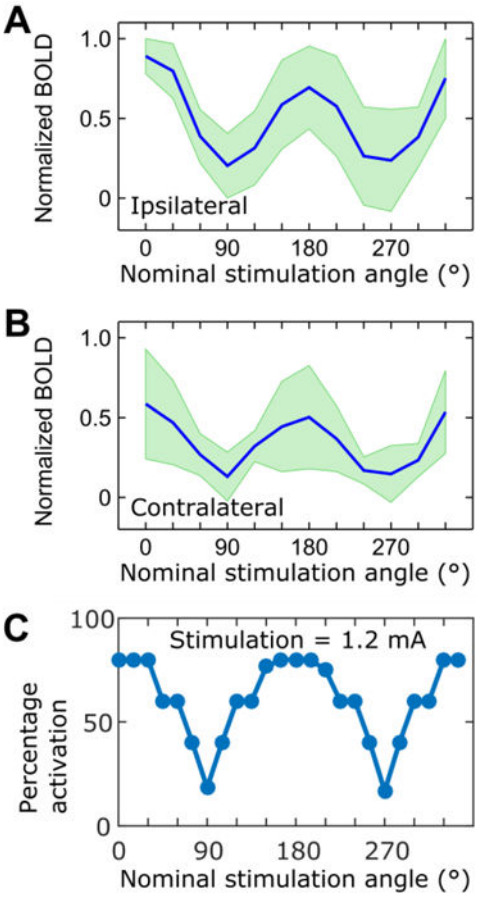

Figure 4.

Dependence of the (A) ipsilateral and (B) contralateral mean BOLD contrast on the nominal stimulation angle. Maximal BOLD contrast was observed for the orientation of 0° between the electric field and CC fibers, while reduced activation was detected upon re-orientation of the electric field anti-parallel (180°) to the axonal tracks; (C) Activation percentages for simulated axons placed radially below the tripolar electrode using a stimulation current of 1.2 mA. See Fig. 2 for the detailed description of the axon placement. SDs are indicated in green (n = 12).

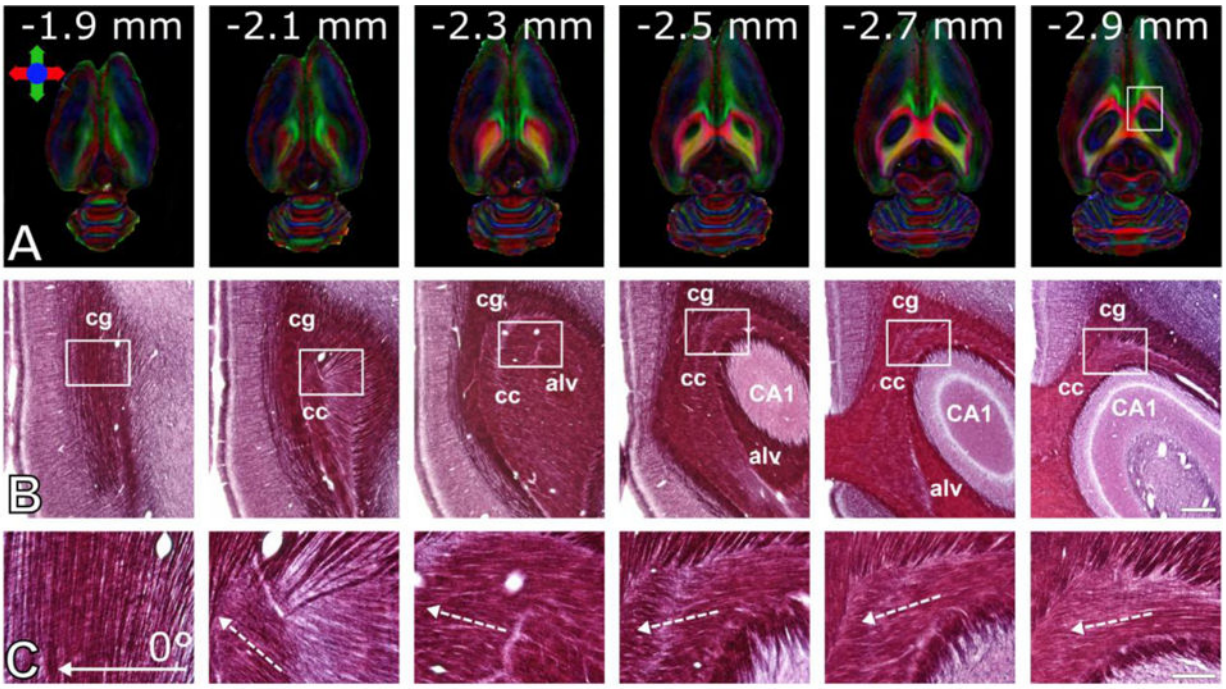

Figure 5.

Variability of axonal directions in a rat. (A) Horizontal slices of directionally encoded color-fractional anisotropy maps obtained using DTI. Colors indicate principle directions of the water diffusion. Numbers indicate the distance of the images from the brain surface. (B) Photomicrographs of myelin stained sections of the same rat brain shown in panel (A). White rectangles represent the frames of the high magnification photomicrographs shown in panel C. Full arrow indicates the stimulation angle 0° used in the experiments, dashed arrows indicate direction of the axons. Abbreviations: cc = corpus callosum, cg = cingulum, alv = alveus, CA1 = hippocampal area CA1. Scale bars: 500 μm (B) and 150 μm (C).

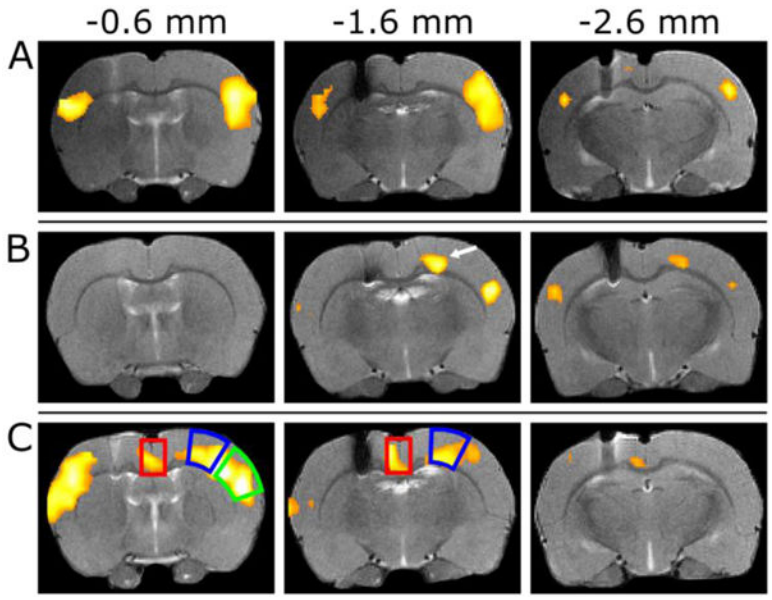

Figure 6.

Examples of the variability of BOLD response at nominal stimulation angle 0°. Representative example with (A) strong activation in $S1_{BF}$, (B) relatively weak activation with BOLD contrast observed in the motor cortex as indicated by an arrow, and (C) strong bilateral activation in the $S1_{BF}$ area, but also with an activation detected in the retrosplenial/cingulate cortices ($Cg_{1/2}$). The smaller activated area ipsilateral to the electrode in (A) is due to the susceptibility artefact in SE-EPI. The red and blue boxes indicate the ROIs used for the results in Table 1 ($Cg_{1/2}$ and $S_{1FL/HL}$, respectively) and the green box indicates the ROI of $S1_{BF}$. The anterior-posterior coordinates are indicated above with −1.6 mm matching to Paxinos' atlas [16].

Table 1

Mean BOLD response of ipsilateral $S1_{BF}$ (also see Figure 4), contralateral $S_{1FL/HL}$ and bilateral $Cg_{1/2}$ at the same nominal stimulation angles.

	BOLD(%), mean ± SD			
	Nominal stimulation angle			
Brain area	**0°**	**90°**	**180°**	**270°**
$S1_{BF}$ (n = 12)	4.5 ± 1.4	0.9 ± 1.0	3.4 ± 1.5	0.9 ± 1.2
S1FL/HL (n = 4)	4.3 ± 0.9	1.2 ± 0.4	2.8 ± 1.9	1.6 ± 0.2
$Cg_{1/2}$ (n = 3)	3.4 ± 0.5	2.0 ± 1.8	1.8 ± 0.1	1.0 ± 0.7